DOI：10.3969/j.issn.2095-1973.2015.01.004
“卫星资料应用” 专题系列

极轨气象卫星高光谱红外探测仪简介

殷梦涛[1] 邹晓蕾[1, 2]
（1 佛罗里达州立大学地球海洋科学大气科学系，美国；2 南京信息工程大学资料同化研究与应用中心，南京 210044）

极轨（polar-orbiting）气象卫星在离地球高度约800km的极地轨道上运行，每天可绕地球14圈，每绕地球一圈需100多分钟。极轨卫星由南到北的地迹线与赤道的交点称为降交点，由北到南的地迹线与赤道的交点称为升交点。极轨卫星不同轨道的地迹线过赤道的经度由于地球自转而不同，但它们经过赤道的地方时间是相同的。一颗极轨气象卫星每天可覆盖全球两次，提供多光谱范围的微波、红外、可见光等全球资料。这与静止（geostationary）卫星不同。静止卫星观测虽然在时间上是连续的，但观测的空间范围和光谱范围有限[1]。极轨气象卫星资料在数值天气预报、气候研究及气象产品反演等领域都有重要应用价值。

搭载有红外探测仪的极轨气象卫星轨道分晨昏轨道、上午轨道及下午轨道三种。晨昏轨道和上午轨道指卫星的降交点时间分别在06:00和10:00左右，下午轨道指卫星的升交点时间在13:00左右①。美国自1978年起发射了美国国家海洋和大气管理局（NOAA）系列极轨环境卫星（POES）。其中NOAA-13在预定下午轨道上运行失败，NOAA-6/8/10/12/15为晨昏轨道卫星，NOAA-17为上午轨道卫星，其余的NOAA系列极轨环境卫星包括NOAA-18/19和Suomi NPP为下午轨道卫星。欧洲气象卫星中心（EUMETSAT）自2006年起已发射的两颗极轨气象业务卫星MetOp-A/B为上午轨道卫星。中国自2008年开始发射风云第3代系列极轨气象卫星 （FY-3），至今已发射了两颗试验气象卫星FY-3A/B和一颗业务气象卫星FY-3C。其中FY-3A/C为上午轨道卫星，分别于2008年5月和2013年9月发射。FY-3B为下午轨道卫星，于2010年11月发射。中国计划在2018年发射本国第一颗晨昏轨道卫星FY-3E，以实现全天候、全球范围的极轨气象卫星观测。表1列出了目前在轨运行的极轨气象卫星的名称、发射时间、红外探测仪、状态及所属机构。

收稿日期：2014 年 8 月 25 日；修回日期：2014 年 11 月 10 日
第一作者：殷梦涛（1991—），Email：my11g@my.fsu.edu
通信作者：邹晓蕾（1960—），Email：xzou@fsu.edu
资助信息：公益性行业（气象）科研专项（GYHY201406008）

第一代高分辨率红外探测仪（HIRS）搭载在1975年发射的Nimbous-6卫星上。当时的HIRS只有16个红外通道和1个可见光通道，之后搭载在NOAA-6～19卫星上的第二、三和四代HIRS （HIRS/2/3/4）有19个

表1 目前在轨运行的极轨气象卫星
Table 1 Current operational polar-orbiting meteorological satellites with their launch dates, infrared sounders, status and agencies

卫星名称	卫星发射时间	卫星红外探测仪	卫星状态	卫星所属机构
NOAA-15	1998-05-13	HIRS/3	业务运行	NOAA
NOAA-18	2005-05-20	HIRS/4	业务运行	NOAA
NOAA-19	2009-02-06	HIRS/4	业务运行	NOAA
Suomi-NPP	2011-10-28	CrIS	业务运行	NOAA
EOS-Terra	1999-12-18	—	业务运行	NASA
EOS-Aqua	2002-05-04	AIRS	业务运行	NASA
EOS-Aura	2004-07-15	—	业务运行	NASA
MetOp-A	2006-10-19	IASI	业务运行	欧洲气象卫星中心
MetOp-B	2012-09-17	IASI	业务运行	欧洲气象卫星中心
FY-3A	2008-05-27	IRAS	业务运行	中国气象局
FY-3B	2010-11-04	IRAS	业务运行	中国气象局
FY-3C	2013-09-23	IRAS	业务运行	中国气象局

表2 第一代HIRS和HIRS/2/3/4的通道中心波数及波段宽度
Table 2 The central wavenumber and the beam width at each channel of the first HIRS and HIRS/2/3/4 cm^{-1}

通道中心波数 HIRS	通道波段宽度 HIRS	通道中心波数 HIRS/2/3/4	通道波段宽度 HIRS/2/3/4
666.67	2.8	668.90	3
680.27	13.7	679.81	10
694.44	12.6	690.13	12
704.23	15.9	703.23	16
714.29	17.5	715.82	16
735.29	17.6	733.14	16
746.27	18.4	749.06	16
909.09	34.6	801.92	16
1219.51	63.4	900.09	35
1492.54	87.6	1029.87	25
2188.18	20.6	1364.26	40
2212.39	22.5	1533.74	55
2242.15	21.6	2188.18	23
2272.73	35.2	2212.39	23
2358.49	23.0	2237.14	23
2695.42	297	2247.19	23
14492.75	892	2421.31	28
—	—	2500.00	35
—	—	2659.57	100
—	—	14492.75	1000

红外通道和1个可见光通道。表2列出了第一代HIRS与HIRS/2/3/4的通道中心波数及波段宽度。与第一代HIRS相比，HIRS/2/3/4没有1219.51cm^{-1}附近的通道，但新增了4个红外通道，这些通道的中心波数分别为801.92、1029.87、1364.26和 2500.00cm^{-1}。

自2002年起搭载在极轨气象卫星上的红外探测仪是新式的高光谱红外探测仪。 至今已提供和正在提供全球观测资料的高光谱红外探测仪包括搭载在美国国家航空航天管理局（NASA）Aqua卫星上的大气红外探测仪（AIRS）、搭载在MetOp-A/B卫星上的红外大气探测干涉仪（IASI）以及搭载在Suomi NPP卫星上的跨轨扫描红外探测仪（CrIS）。显然，三种不同高光谱红外探测仪AIRS、IASI和CrIS比高分辨率红外探测仪（HIRS系列）的光谱分辨率高得多。AIRS在650～2700cm^{-1}范围内有2378个通道，IASI在600～2800cm^{-1}范围内有8461个通道。CrIS在650～2550cm^{-1}范围内有1305个通道，分长波、中波及短波三个波段，这三个波段的观测范围分别为650～1095cm^{-1}、1210～1750cm^{-1}及2155～2550cm^{-1}②。而HIRS/2/3/4在650～2700cm^{-1}范围内只有19个通道。这三种高光谱红外探测仪具有不同的光谱分辨率。AIRS的光谱分辨率（$\Delta\nu$）随着通道中心波数（ν）的增加而增加，与恒定的光谱分辨系数（R）成反比[2]，即：

$$R = \frac{\nu}{\Delta\nu}, \qquad (1)$$

式中，R=1200。IASI在全波段范围内具有恒定的光谱分辨率0.25cm^{-1}。CrIS在长波、中波及短波三个波段内分别具有恒定的光谱分辨率0.625、1.25及2.5cm^{-1}②。利用全波段分辨率模式，CrIS在全波段范围内的光谱分辨率为0.625cm^{-1}[3]。Strow等[4]发现由于CrIS短波波段的光谱分辨率比IASI短波波段的光谱分辨率低得多，无法在卫星升空后用IASI短波资料对CrIS短波波段进行绝对频率订正。在全波段分辨率模式下，CrIS可以提供高光谱分辨率的短波资料，实现CrIS短波波段的绝对频率订正[5]。

下面以最新高光谱红外探测仪CrIS为例，进一步讨论高光谱红外探测仪的其他主要特点。CrIS是跨轨扫描仪器，它在单条扫描线上的能视场（Field of Regard，FOR）数为30，每个能视场又由9个瞬时视场（Field of View，FOV）组成。当卫星Suomi NPP自南向北沿轨运行时，高光谱红外探测仪CrIS自西向东跨轨观测30个能视场。CrIS资料的水平分辨率主要由波束宽度决定，也与扫描角及卫星高度有关。CrIS的波束宽度为0.963°，对应星下点资料的瞬时视场直径为14km。图1展示了赤道附近一条CrIS扫描线上瞬时视场和能视场大小分布。图中瞬时视场和能视场的轨迹是根据CrIS瞬时视场中心的经纬度、仪器波束宽度及Suomi NPP卫星天顶角、方位角、高度计算得到的。计算细节见附录。由图1知，瞬时视场和能视场面积随扫描角增大而增大，即跨轨扫描仪器CrIS资料的水平分辨率在星下点处最大，随扫描角增大而减小。当扫描角较大时，CrIS能视场在跨轨方向有重叠。图2放大展示了一条CrIS扫描线上能视场1、15、30内9个瞬时视场的分布。选择的单条CrIS扫描线与图1一样。每个能视场内，瞬时视场5被称为中心瞬时视场（Center FOV），瞬时视场1、3、7、9被称为对角瞬时视场（Corner FOV），瞬时视场2、4、6、8被称为邻边瞬时视场（Side FOV）[3]。对于单条扫描线来说，对角瞬时视场和邻边瞬时视场的位置绕着中心瞬时视场自西向东逆时针旋转。由图2可见，同一能视场内的9个瞬时视场之间无重叠。

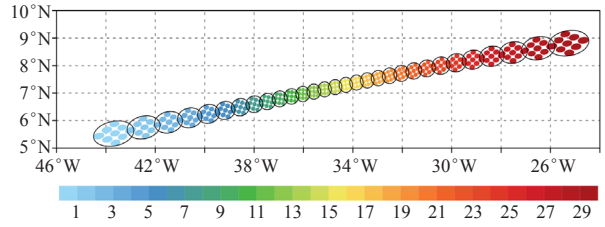

图1 赤道附近一条CrIS扫描线上瞬时视场和能视场大小分布，不同能视场内的9个瞬时视场由不同颜色表示

Fig. 1 The sizes and distributions of FOVs and FORs for a single scanline of CrIS near the equator. The 9 FOVs within different FOR are indicated by different colors

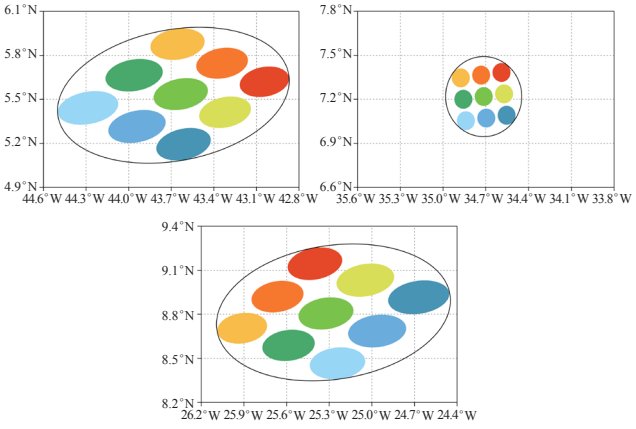

图2 一条CrIS扫描线上放大的能视场内9个瞬时视场的分布（选择的单条CrIS扫描线与图 1一样）

Fig. 2 The enlarged 9 FOVs of FORs 1, 15 and 30 for the same scanline of CrIS as in Fig. 1

图3展示了CrIS 9个瞬时视场的跨轨直径和沿轨直径随能视场的变化。选择的单条CrIS扫描线与图1

一样。值得注意的是，随着扫描角增大，9个瞬时视场跨轨视场直径比沿轨视场直径增大得更明显。在星下点处，跨轨视场直径比沿轨视场直径稍小，这是因为瞬时视场在沿轨方向经历了更大的纬向扭曲。这里，纬向扭曲指地球半径从赤道（6378.1km）到极地（6356.8km）逐渐减小，导致极轨卫星离地球表面的距离随纬度增加而增加，因而同一仪器在高纬观测的瞬时视场面积比在低纬时大。在最大扫描角处，9个瞬时视场的最小跨轨直径约为39km，而9个瞬时视场的最大沿轨直径约为25km。

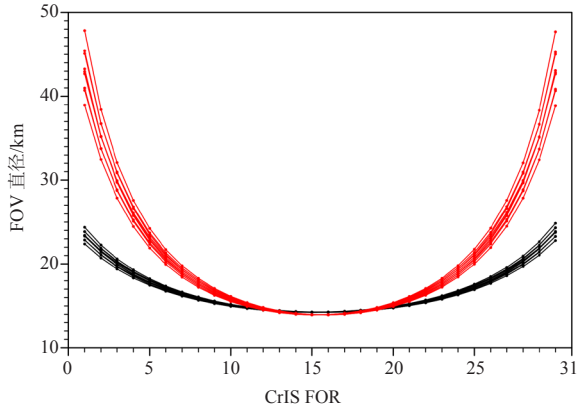

图3 CrIS 9个瞬时视场跨轨直径（红色）和沿轨直径（黑色）随能视场的变化（选择的单条CrIS扫描线与图 1一样）
Fig. 3 The cross-track and along-track diameters of 9 FOVs along the same scanline of CrIS as in Fig. 1

与CrIS类似，HIRS和AIRS都是跨轨扫描仪器。第一代HIRS在每条扫描线上有42个瞬时视场，HIRS/2/3/4在每条扫描线上有56个瞬时视场。AIRS在每条扫描线上有90个瞬时视场。值得注意的是，每代HIRS的星下点水平分辨率都不相同。第一、二代高分辨率红外探测仪HIRS和HIRS/2的星下点水平分辨率分别为25和17.7km。第三代高分辨率红外探测仪HIRS/3在可见光和短波红外通道的星下点水平分辨率均为20.3km, 但在长波红外通道的星下点水平分辨率略有不同，为18.9km。第四代高分辨率红外探测仪HIRS/4的星下点水平分辨率为10km，比前三代HIRS仪器的星下点水平分辨率差不多高一倍。AIRS的星下点水平分辨率为13.5km。图4a—4c比较了HIRS/3长波红外通道、AIRS及CrIS在星下点附近的瞬时视场大小分布。由图可知，在扫描角相同的条件下，HIRS/3红外长波通道的瞬时视场最大，AIRS的瞬时视场最小，CrIS的瞬时视场大小居中。HIRS/3红外长波通道、AIRS和CrIS的瞬时视场大小差异主要是由这三种仪器的波束宽度差异造成的，与卫星高度差异也有关。HIRS/3红外长波通道、AIRS和CrIS的波束宽度分别为1.3、1.1和0.963°。搭载AIRS的Aqua卫星高度仅为705km，搭载CrIS的Suomi NPP卫星高度为834km。虽然AIRS的波束宽度大于CrIS的波束宽度，但由于Aqua卫星高度低于Suomi NPP卫星高度，AIRS的瞬时视场比CrIS的瞬时视场小。在星下点附近，三种仪器在跨轨和沿轨方向均无视场重叠，HIRS/3长波红外通道的瞬时视场在跨轨和沿轨方向均有较大间隙，AIRS的瞬时视场只在沿轨方向有较小间隙，CrIS的瞬时视场在跨轨和沿轨方向的间隙都较小。

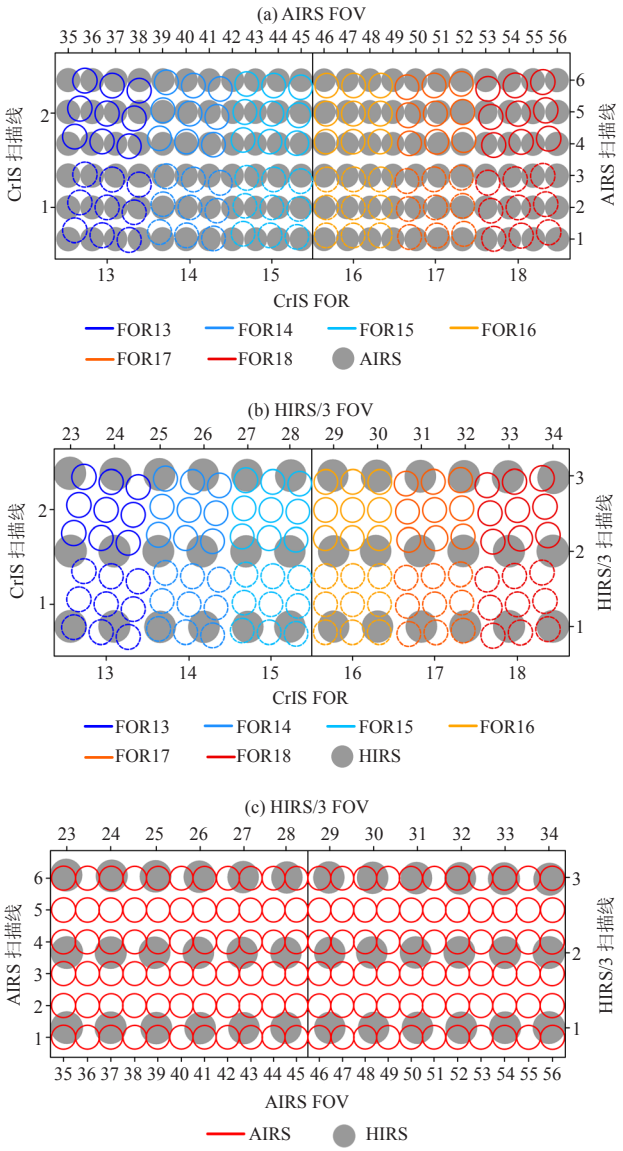

图4 星下点附近瞬时视场大小分布和比较
Fig. 4 The comparison of sizes and distributions of FOVs between (a) AIRS and CrIS, (b) infrared longwave channels of HIRS/3 and CrIS as well as (c) infrared longwave channels of HIRS/3 and AIRS near nadir

在晴空条件下，忽略散射项，CrIS观测到的辐射是一段时间里，由波束宽度决定的锥形体积内，由权

重函数决定的一定高度范围里的大气红外辐射总量。CrIS观测单个能视场内9个瞬时视场的时间为0.2s[3]。CrIS提供了655～2550cm^{-1}范围内1305个通道的亮温资料，但过多的通道导致部分通道观测的红外辐射会来自相同高度范围。因此，CrIS全通道辐射资料里包含了很多重复信息。在数值天气预报中，为了减少计算量和不同通道之间的相关，满足业务资料同化和反演的需求，有必要对CrIS的1305个通道进行筛选。CrIS的通道筛选有两个大原则。一个是优先选择只对特定大气物理量敏感的通道，这样可以有效避免不同通道包含重复冗长的信息；另一个是优先选择垂直分辨率更高的通道，这样可以提高反演产品的垂直分辨率[6]。CrIS的垂直分辨率由各通道的权重函数决定。某通道的权重函数垂直分布越窄，则该通道的垂直分辨率越高。权重函数最大值所在高度的大气对该通道观测的辐射量值贡献最大[7]。不同通道的权重函数最大值分布在不同高度，这是反演大气物理量垂直廓线的基础。此外，CrIS的通道筛选也要考虑所选通道的垂直观测范围。Gambacorta等[6]根据以上原则从CrIS 1305个通道中选出了399个通道，用于数值天气预报的同化系统中。这些通道包括24个地表温度通道、87个大气温度通道、62个水汽通道、53个O_3通道、27个CO通道、54个CH_4通道、52个CO_2通道、24个N_2O通道、28个HNO_3通道和24个SO_2通道。图5a—5d分别展示了美国标准大气条件下利用通用辐射传输模式（CRTM）[8]计算得到的CrIS红外长波温度通道、红外短波温度通道、水汽通道和地表温度通道的权重函数垂直分布。红外长波、中波及短波通道分别由蓝、绿及红色表示。图6展示了这399个CrIS通道权重函数最大值高度分布。由图5和图6知，温度通道分布在660～750cm^{-1}和2200～2420cm^{-1}光谱范围内。其中红外长波温度通道（660～750cm^{-1}）紧密排列在1000～10hPa左右的垂直范围内，可提供高垂直分辨率的大气温度垂直廓线。红外短波温度

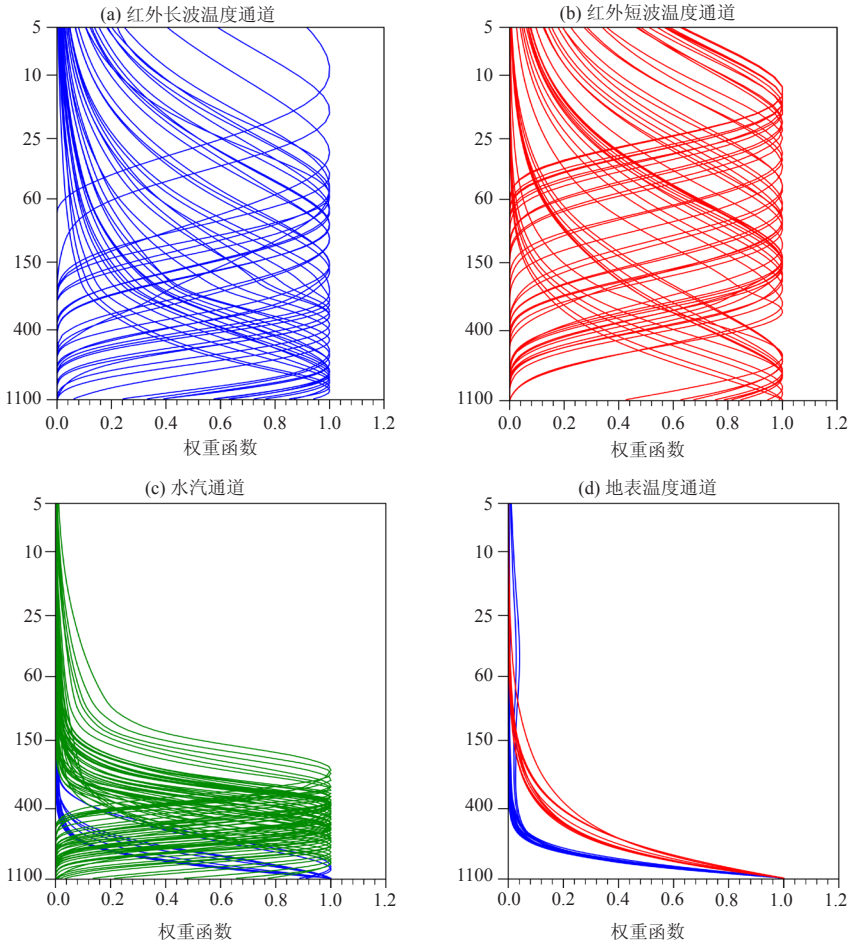

蓝色：红外长波通道；绿色：中波通道；红色：短波通道

图5 美国标准大气条件下利用CRTM计算得到的CrIS的权重函数垂直分布

Fig. 5 The weighting function distributions of CrIS (a) longwave infrared, (b) shortwave infrared, (c) water vapor and (d) surface temperature channels calculated by the CRTM under the US standard atmosphere

通道（2200～2420cm^{-1}）的垂直分布与红外长波温度通道类似，但在60～10hPa左右的垂直范围内排列更紧密，可提供更多的高空大气温度信息。臭氧通道分布在990～1070cm^{-1}光谱范围内。臭氧的强振动吸收带位于1041.67cm^{-1}附近，90%的臭氧集中在平流层10～50km，剩下的10%集中在地表附近③。水汽通道分布在780～1210cm^{-1}和1310～1750cm^{-1}光谱范围内。其中红外长波水汽通道（780～1210cm^{-1}）可提供地表附近的水汽分布信息。红外中波水汽通道（1310～1750cm^{-1}）紧密排列在800～200hPa左右的垂直范围内，可提供高垂直分辨率的大气水汽垂直廓线。地表温度通道分布在770～1095cm^{-1}和2460～2540cm^{-1}光谱范围内。值得注意的是，红外短波地表温度通道（2460～2540cm^{-1}）因为有可能受反射的太阳光污染影响，目前还没有在美国国家环境预报中心（NCEP）数值天气预报系统中得到使用[9]。

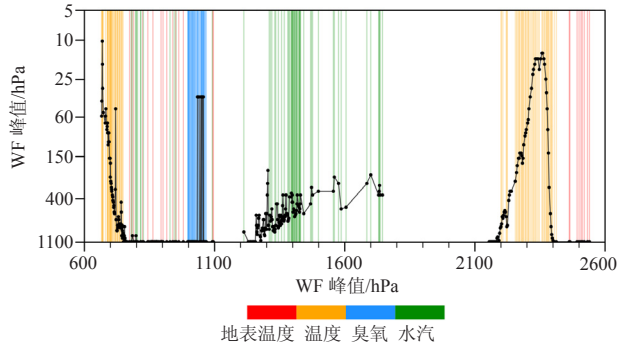

图6 CrIS 399个通道权重函数最大值高度分布（黑色实线和点）

Fig. 6 The distributions of altitudes of weighting function peaks for CrIS 399 channels (black solid lines with circles). Surface temperature, temperature, ozone and water vapor channels are indicated by red, orange, blue and green solid lines

飓风“桑迪”在2012年10月25日06时（世界时）左右登陆古巴④。图7a展示了该时刻NCEP再分析（FNL）资料提供的海平面气压和地表温度；图7b—7c展示了该时刻Suomi NPP降轨方向CrIS红外长波地表温度通道79的观测亮温。由图7a知，飓风“桑迪”位于暖洋面上，其中心气压低于998hPa。与微波辐射相比，红外辐射的波长较短，在云中衰减更快。如果云的光学厚度较大，CrIS通道79观测的辐射主要来自云顶，否则来自地表。由图7b知，有云区域的亮温可以低于195K，无云区域的亮温可以高于295K。飓风中心与周围环境具有明显的温差，飓风眼区的亮温可以高于260K，而周围环境的亮温可以低于200K。这反映了飓风中心为暖核，眼墙区及眼墙外有厚云的一个结构。图8a展示了CrIS 11个红外长波温度通道的权重函数垂直分布；图8b展示了同一时刻这11个通道通过飓风中心、沿着轨道方向由南向北的观测亮温垂直结构。由图8b知，在同一高度上，飓风中心温度最高；在同一纬度上，飓风中心在地表的温度最高。在地表附近，飓风中心与周围环境的温差可以高达60K。CrIS红外长波温度通道很好地捕捉到了飓风“桑迪”的水平和垂直结构。

较早的高光谱红外探测仪AIRS和IASI已经在数值天气预报同化系统中得到广泛应用。McNally等[10]设计了两个实验来研究AIRS晴空资料同化效果。第一个实验是在欧洲中尺度天气预报中心（ECMWF）四维变分系统里单独同化AIRS、AMSU-A和HIRS晴空资料，发现AIRS晴空资料对模式预报场的改进效果要好于光谱分辨率较低的AMSU-A和HIRS晴空资料；第二个实验是在ECMWF业务同化系统里增加AIRS晴空资料，发现增加AIRS晴空资料对ECMWF业务预报仍然有正效果。Guidard等[11]研究了IASI晴空和有云资料同化对数值天气预报的影响，发现IASI晴空资料对模式预报场有明显改进，而IASI有云资料对模式预报场几乎没有改进。这是因为IASI有云资料同化需要高精度的云参数，而目前还没有一种有效的方法可以得到高精度的云参数。作为最新的高光谱探测仪，CrIS在数值天气预报领域的应用还有待进一步的研究。另一方面，三种高光谱红外探测仪都已经被应用在气象产品反演和气候研究领域。AIRS与先进微波探测仪（AMSU）在2002年组成AIRS/AMSU反演产品处理系统；IASI、AMSU与微波湿度探测仪（MHS）在2008年组成IASI/AMSU/MHS微量气体产品处理系统；CrIS与先进技术微波探测仪（ATMS）在2013年组成CrIS/ATMS处理系统。Gambacorta等[12]用NOAA卫星应用和研究中心（STAR）业务高光谱反演算法比较了AIRS/AMSU、IASI/AMSU/MHS和CrIS/ATMS三种系统反演产品的精度。该研究指出CrIS/ATMS系统可以提供与另两种系统反演产品精度接近的大气温度和水汽垂直廓线，但CrIS/ATMS系统提供的低对流层温度廓线和中对流层水汽廓线与另两种系统对应的反演产品有较大出入。此外，利用CrIS全光谱模式（全波段光谱分辨率为0.625cm^{-1}）的CrIS/ATMS系统可以提供与另两种系统反演产品精度接近的大气CO垂直廓线。总体来讲，CrIS/ATMS处理系统基本满足了气象产品反演和气候研究的要求。只有对CrIS资料的偏差订正、质量控制、云检测和反演算法等进行一系列更深入细致的研究，才能在数值天气预报、气象产品反演和气候研究领域充分发挥CrIS提供的高光谱红外资料的作用。

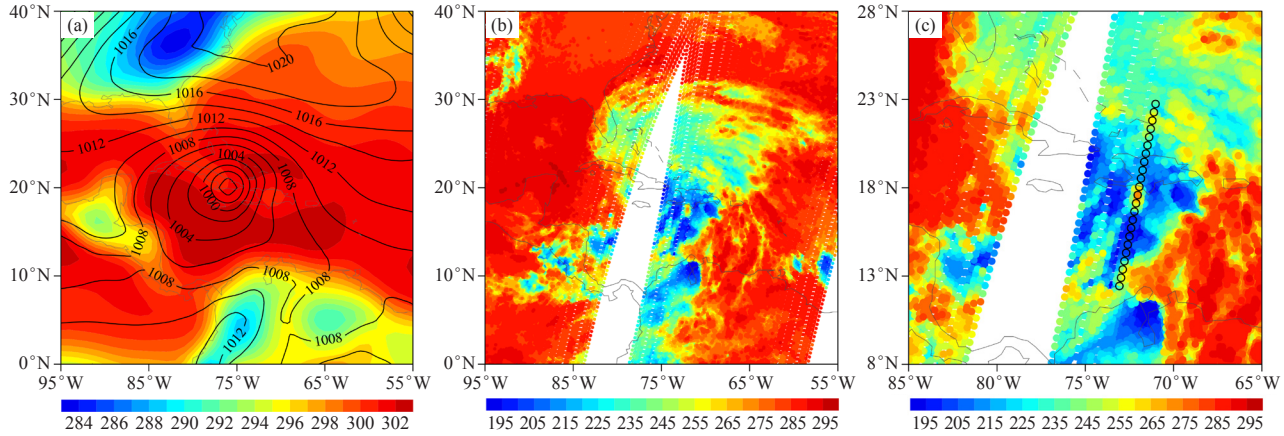

图7 （a）2012年10月25日06时（世界时）NCEP FNL资料提供的海平面气压（等值线，hPa）和地表温度（填色，K）；（b）同一时刻Suomi NPP降轨方向CrIS通道79的观测亮温（散点， K）(c与b相同，但所选区域更小）

Fig. 7 (a) The sea level pressure and sea surface temperature of NCPE Final (FNL) global analysis at 0600 UTC 25 October 2012, (b) the observed brightness temperature of CrIS infrared longwave surface temperature channel 79 from the descending node of Suomi NPP at the same moment and (c) the same as (b) except over a smaller domain

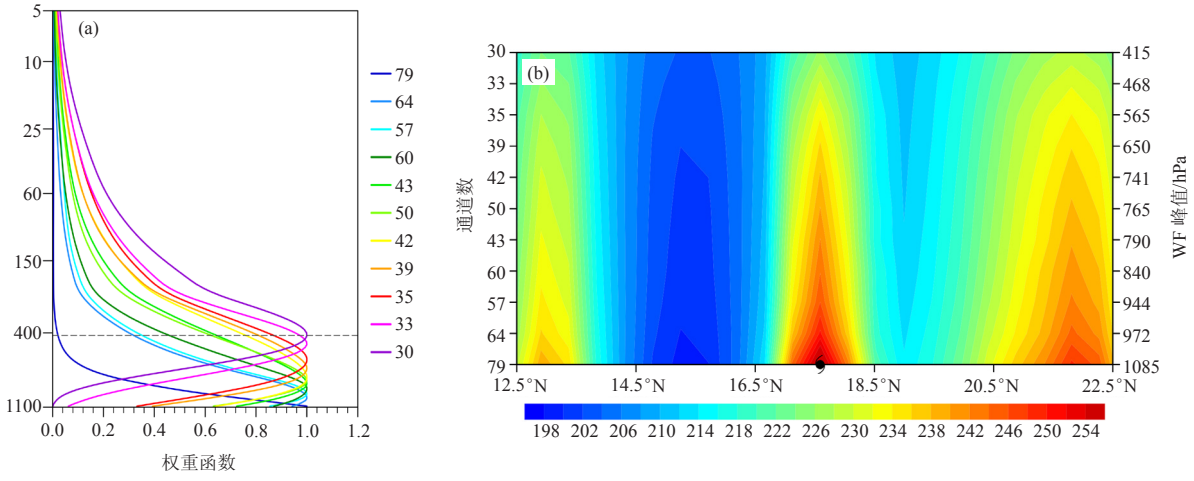

图8 （a）美国标准大气条件下利用CRTM计算得到的CrIS 11个红外长波温度通道的权重函数垂直分布，415hPa所在高度由灰色虚线表示；（b）2012年10月25日06标准时这11个通道通过飓风中心、沿着轨道方向由南向北的观测亮温垂直结构（填色，K）（选择的资料为CrIS降轨方向第28个能视场内的中心瞬时视场（图6c的黑色圆圈））

Fig. 8 (a) The weighting function distributions of CrIS 11 infrared longwave temperature channels calculated by CRTM under the US standard atmosphere. The altitude of 415 hPa is indicated by a gray dash line. (b) The cross section of brightness temperatures for CrIS 11 infrared longwave temperature channels through the hurricane center in the along–track direction from the ascending node of Suomi NPP at 0600 UTC 25 October 2012. The selected observations are along the center FOV of the 28th FOR (black circle in Figure 6c)

Serial of Applications of Satellite Observations

An Introduction to Hyper-spectral Infrared Sounders Onboard Polar-orbiting Meteorological Satellites

Yin Mengtao[1] Zou Xiaolei[1, 2]

(1 Department of Earth, Ocean and Atmospheric Science, Florida State University, USA
2 Center of Data Assimilation for Research and Application, Nanjing University of Information and Science & Technology, Nanjing 210044)

Polar-orbiting meteorological satellites circulate above the Earth at about 800-km altitude, completing 14 orbits daily. A single orbit takes about 100 minutes. Each polar-orbiting satellite provides observations on the so-called descending (ascending) node when moving from north (south) to south (north). The local time for all the descending nodes to cross the equator remains constant for a fixed polar-orbiting satellite, although their longitudes are different. The same is true of ascending nodes. Different from a geostationary satellite that provides temporally continuous observations within a limited spatial and spectral domain[1], a polar-orbiting meteorological satellite can provide global coverage in multiple visible, infrared and microwave bands twice daily. Observations from polar-orbiting meteorological satellites have played important roles in numerical weather prediction (NWP), climate study and product retrieval of meteorological variables.

Polar-orbiting meteorological satellites with infrared sounders onboard are launched into early-morning, morning and afternoon orbits. The descending nodes of early-morning and morning orbits pass the equator at about 6:00 AM and 10:00 AM local equatorial crossing time (LECT), respectively. The LECT of ascending nodes of afternoon orbits is at about 1:00 PM local time①. National Oceanic and Atmospheric Administration (NOAA) started its Polar Orbiting Environmental Satellite (POES) series in 1978. NOAA-13 failed to operate in an afternoon orbit. NOAA-6/8/10/12/15 are early-morning satellites. NOAA-17 is a morning satellite. The remaining NOAA POES, including NOAA-18/19 and Suomi NPP, are afternoon satellites. Other countries also operated polar-orbiting meteorological satellites. Other countries also operated polar-orbiting meteorological satellites. Two morning-orbiting satellites MetOp-A/B has been launched by European Organization for the Exploitation of Meteorological Satellites (EUMETSAT) since 2006. The Chinese Fengyun-3 (FY-3) polar-orbiting meteorological satellite series started from 2008 on. FY-3A/B are experimental meteorological satellites, and FY-3C is an operational meteorological satellite. FY-3A/C are morning satellites and were launched in May 2008 and September 2013, respectively. FY-3B is an afternoon satellite and was launched in November 2010. China plans to launch an early-morning-orbiting satellite, FY-3E, in 2018. By then, the FY-3 satellites will provide global observations with three different orbits, i.e., early-morning, morning and afternoon orbits. Table 1 provides a list of the current operational polar-orbiting meteorological satellites with their launch dates, infrared sounders, status and agencies.

The first High-resolution Infrared Radiometer Sounder (HIRS) was onboard Nimbous-6 satellite, which was launched in 1975. HIRS had 16 infrared channels and one visible channel. The follow-up HIRS instruments, HIRS/2/3/4 onboard the NOAA-6 to 19 had 19 infrared and one visible channel. Table 2 lists the central wavenumbers and the bandwidth at each channel of the first HIRS and HIRS/2/3/4. It is seen that the 1219.51 cm^{-1} channel of the first HIRS was removed from HIRS/2/3/4. Four new infrared channels were added to HIRS/2/3/4 with their central wavenumbers at801.92, 1029.87, 1364.26 and 2500.00 cm^{-1}, respectively.

Hyper-spectral infrared sounders, include Atmospheric Infrared Sounder (AIRS) onboard the National Aeronautics and Space Administration (NASA) Aqua satellite since 2002, Infrared Atmospheric Sounding Interferometer (IASI) onboard MetOp-A/B satellite, and Cross-track Infrared Sounder (CrIS) onboard Suomi NPP satellite since 2010, represent the advancement in infrared sounding technology. The spectral resolutions of AIRS, IASI and CrIS are much higher than HIRS instruments. AIRS has 2378 channels covering a spectral range from 650 to 2700 cm^{-1}. IASI provides radiance measurements with 8461 channels that are located in a spectral range from 600 to 2800cm^{-1}. CrIS provides radiance measurements at a total of 1305 channels, which are divided into longwave (650 to 1095 cm^{-1}), midwave

(1210 to 1750 cm^{-1}) and shortwave (2155 to 2550 cm^{-1}) bands②. HIRS/2/3/4 only provide radiance measurements at 19 channels from 650 to 2700 cm^{-1}. The above three hyper-spectral infrared sounders have different spectral resolutions. The spectral resolution (Δv) of AIRS increases with increasing central wavenumber (v) and is inversely proportional to a constant spectral resolving power (R) [2], i.e.:

$$R = \frac{v}{\Delta v}, \quad (1)$$

where R=1200. IASI has a constant spectral resolution of 0.25cm^{-1} over its entire observing spectral range. CrIS has a constant spectral resolution at each of its three spectral bands. The spectral resolutions of longwave, midwave and shortwave bands are 0.625, 1.25and 2.5 cm^{-1}, respectively. The full spectral resolution (FSR) mode allows CrIS to have a spectral resolution of 0.625 cm^{-1} over the full spectral range of CrIS [3]. The spectral resolution of CrIS shortwave band is much coarser than that of the corresponding IASI band. It was found to be difficult to apply the absolute frequency calibration in the CrIS shortwave band by employing IASI shortwave observations during the post-launch period due to the differences of spectral resolutions between two instruments [4]. By utilizing the FSR mode, the absolute frequency calibration in the CrIS shortwave band becomes straightforward using IASI [5].

CrIS is the newest hyper-spectral infrared sounder and will be taken as an example for further discussions. CrIS is a cross-track scanning instrument. A single scanline of CrIS consists of 30 fields of regard (FORs), with each FOR consisting of nine fields of view (FOVs). As the satellite Suomi NPP moves in the along-track direction from South to North, the hyper-spectra infrared sounder CrIS observed 30 FORs in the cross-track direction from West to East. The horizontal resolution of CrIS observations is determined mainly by the beam width. The scan angle and the altitude of satellite also have an impact on CrIS data resolution. The beam width for CrIS is 0.963°, corresponding to an FOV with a 14-km diameter at nadir. The sizes and distributions of FOVs and FORs along a single scanline of CrIS near the equator are shown in Figure 1. The footprints of the FOV and the FOR in the figure were calculated based on the center longitude and latitude of a particular FOV, the beam width as well as the zenith angle, the azimuth angle and the altitude of Suomi NPP satellite. A detailed description of the mathematical formula for the calculation of FOR and FOV sizes can be found in the appendix. From Figure 1 it is seen that the sizes of the FOV and the FOR increase with scan angle, confirming that the horizontal resolution of CrIS observations is the highest at nadir and decreases with an increasing scan angle. An overlap is found for CrIS FOVs with large scan angles in the cross-track direction. An enlarged view of the nine FOVs for FORs 1, 15 and 30 in Figure 1 are displayed in Figure 2. FOV 5 is the center FOV, FOVs 1, 3, 7 and 9 are corner FOVs, and the FOVs 2, 4, 6 and 8 are side FOVs [3]. The corner and side FOVs rotate around the center FOV counter-clockwise from the west to the east for a single scanline. It is reminded that there is no overlap between neighboring FOVs within a single FOR.

The cross-track and along-track diameters of the nine FOVs along the same scanline of CrIS in Figure 1 are provided in Figure 3. It is worth noticing that the cross-track diameters of the nine FOVs increase with scan angle more greatly than the along-track diameters. The cross-track diameters are slightly smaller than the along-track diameters at nadir due to a larger latitudinal distortion of the nine FOVs in the along-track direction. The latitudinal distortion is caused by the larger radius of the Earth at the equator (6378.1 km) than at the pole (6356.8 km). It leads to a higher altitude of the Suomi NPP satellite at higher latitudes than low latitudes such that the FOV observed by the CrIS instrument is larger at higher latitudes. At the largest scan angle, the minimum cross-track and maximum along-track diameter of the FOVs is about 39 and 25 km, respectively.

Similar to CrIS, all HIRS series and AIRS are cross-track scanning instruments. There are 42 FOVs and 56 FOVs along a single scanline of the first HIRS and HIRS/2/3/4, respectively. The total number of FOVs for a single scanline of AIRS is 90. It is worth noticing that the horizontal resolution of each generation of HIRS series is different. The horizontal resolution of the first HIRS and HIRS/2 at nadir is 25 and 17.7 km, respectively. The horizontal resolution of visible and infrared shortwave channels of HIRS/3 at nadir is 20.3 km, and that of infrared longwave channels of HIRS/3 is 18.9 km. The nadir resolution of HIRS/4 is 10 km, nearly twice as high as that of the other HIRS instruments. The nadir resolution of AIRS is 13.5 km. A comparison of sizes and distributions of FOVs among AIRS, CrIS and infrared longwave channels of HIRS/3 near nadir is provided in Figure 4. At the same scan angle, the FOV size is the largest for the infrared longwave channels of HIRS/3, the smallest for AIRS, and moderate for CrIS. Differences in FOV sizes of the infrared longwave channels among HIRS/3, AIRS and CrIS arise mainly from differences in the beam widths of the three instruments as well as the altitudes of the corresponding satellite platforms. The beam widths for HIRS/3, AIRS and CrIS are 1.3, 1.1 and

0.963°. The altitude of Aqua satellite with AIRS onboard is 705 km, while the altitude of Suomi NPP satellite with CrIS onboard is 834 km. Although the beam width for AIRS is larger than that for CrIS, the FOV size for AIRS is smaller than that for CrIS due to a lower altitude of Aqua than that of Suomi NPP. Near nadir, no overlaps occur between neighboring FOVs for the three instruments in both cross-track and along-track directions. A large space between neighboring FOVs for the infrared longwave channels of HIRS/3 exists in both the cross-track and along-track directions. A small space between neighboring FOVs is observed in cross-track directions for AIRS and both cross-track and along-track directions for CrIS.

Under clear-sky conditions, the measured infrared radiance comes from a specific volume of the atmosphere, which is determined by the beam width, the weighting function, and the observing time period. A single CrIS FOR consisting of nine FOVs takes about 0.2 s to observe [3]. As is mentioned above, CrIS provide radiance observations at 1305 channels in the spectral range of 655-2550 cm^{-1}. The radiance observations may come from different atmospheric volumes with significant overlaps. Hence, the radiance observations of CrIS full spectral range contain significantly redundant and thus correlated information. In NWP, a channel selection becomes necessary for CrIS data assimilation in order to avoid error correlations between different channels and to reduce the computational expense. The channel selection for CrIS has two main principles: select channels with high sensitivity to a certain atmospheric species and high vertical resolution. The former is to effectively reduce the redundancy between different channels and the latter is to maximize the vertical resolution of the retrieval product [6]. The vertical resolution of CrIS observations is determined by the weighting function of each channel. The narrower the weighting function is, the higher the vertical resolution is for a specific channel. The atmosphere at the altitude of weighting function peak contributes most to the radiance observed by that channel [7]. The weighting functions of different channels reach the maximum at different altitudes, which is the basis for retrieving the vertical profiles of atmospheric species. In addition, the vertical observing range of channels is also considered in the channel selection for CrIS. Gambacorta et al. [6] select a total of 399 CrIS channels for applications in NWP data assimilation system. This subset of CrIS channels includes 24 surface temperature, 87 temperature, 62 water vapor, 53 ozone, 27 carbon monoxide, 54 methane, 52 carbon dioxide, 24 N_2O, 28 HNO_3 and 24 SO_2 sounding channels. Figure 5 presents the weighting function profiles of CrIS longwave infrared, shortwave infrared, water vapor and surface temperature channels calculated by the Community Radiative Transfer Model (CRTM) [8] under the US standard atmosphere. The infrared longwave, midwave and shortwave channels are indicated in blue, green and red colors, respectively. Figure 6 provides the distributions of altitudes of weighting function peaks for the 399 CrIS channels. It is seen that temperature channels are distributed in longwave and shortwave bands. The infrared longwave temperature channels (660 to 750 cm^{-1}) are arranged compactly from 1000 to 10 hPa, providing the vertical profile of atmospheric temperature with high vertical resolution. The infrared shortwave temperature channels (2200 to 2420 cm^{-1}) are arranged in a similar pattern to infrared longwave temperature channels but more compactly in the vertical range of 60 to 10 hPa, which can provide more information about the upper atmospheric temperature. Ozone channels are distributed over the spectral range of 990 to 1070 cm^{-1}. The strong vibrational absorption band of ozone is near1041.67 cm^{-1}. About 90% ozone is concentrated in the stratosphere within the altitude range from 10 to 50 km, and the remaining 10% ozone is concentrated near the Earth's surface③. Water vapor channels are distributed over the following two spectral ranges: 780-1210 cm^{-1} and 1310-1750 cm^{-1}. The longwave water vapor channels (780 to 1210 cm^{-1}) can provide the water vapor information near the surface. The midwave water vapor channels (1310 to 1750 cm^{-1}) are arranged compactly in the vertical range from 800 to 200 hPa, enabling the vertical profiling of the atmospheric water vapor. Surface temperature channels are distributed over two spectral ranges of 770-1095 cm^{-1} and 2460-2540 cm^{-1}. It is worth mentioning that the infrared shortwave surface temperature channels (2460 to 2540 cm^{-1}) are not used in the National Centers for Environmental Prediction (NCEP) NWP systems due to a potential contamination of sun glint [9].

Hurricane Sandy made landfall at Cuba at 0600 UTC October 25, 2012. The sea level pressure and sea surface temperature of NCEP Final (FNL) global analysis at the same time is presented in Figure 7a. The observed brightness temperature of CrIS infrared longwave surface temperature channel 79 from the descending node of Suomi NPP at the same time is provided in Figure 7b and 7c. It is found that Hurricane Sandy is located over a warm sea surface with a low-pressure center of less than 998 hPa (Figure 7a). Compared to microwave, the wavelength of infrared is shorter, implying that the infrared radiance is attenuated in clouds more quickly. If the cloud has a large optical depth, the radiance measured

by CrIS channel 79 mainly comes from the cloud top, otherwise from the Earth surface. The brightness temperatures over cloudy areas are as low as 195 K, while those over clear-sky areas can reach up to 295 K (Figure 7b). A warm anomaly is observed near the Sandy center. The brightness temperatures in Hurricane Sandy's eye are as high as 260 K, in a great contrast to those in the neighboring environment of lower than 200 K. It reflects a typical warm core structure in the hurricane center with thick clouds within and outside the eye wall. Figure 8a presents the weighting function distributions of 11 CrIS infrared longwave temperature channels. The cross section of brightness temperatures for these 11 CrIS infrared longwave temperature channels through the hurricane center in the along-track direction from the ascending node of Suomi NPP at 0600 UTC October 25, 2012 is provided in Figure 8b. It is seen that the brightness temperature reaches the maximum at the surface within the eye. The brightness temperature difference between the hurricane center and the nearby environment is as high as 60 K. The horizontal and vertical structures of Hurricane Sandy are well captured by CrIS infrared longwave temperature channels.

The prior hyper-spectral infrared sounders including AIRS and IASI have been widely used in NWP data assimilation system. McNally et al. [10] designed two experiments to explore the impact of AIRS data assimilation using only clear-sky observations. One experiment was to assimilate the clear-sky radiance from a single instrument (AIRS, HIRS and AMSU-A) in the ECMWF four-dimensional variational data assimilation system. AIRS data assimilation was found to outperform the assimilation of data from other two instruments with lower spectral resolutions (HIRS and AMSU-A). Another experiment was to add AIRS clear-sky observations into the ECMWF operational data assimilation system. It was found that AIRS had a positive impact on ECMWF operational forecasts. Guidard et al. [11] studied the impact of IASI data assimilation using both clear-sky and cloudy observations. The IASI clear-sky measurements were found to improve the model forecasts, while the IASI cloudy measurements had a neutral influence on the model forecasts due to the shortage of an effective method which can retrieve cloud parameters of high precision. The applications of the newest hyper-spectral infrared sounder (CrIS) in NWP have not yet to be demonstrated. On the other hand, all three hyper-spectral infrared sounders have been applied in the retrieval of meteorological variables and climate research. The AIRS/Advanced Microwave Sounding Unit (AMSU) retrieval product processing system has been running since 2002. IASI, AMSU and Microwave Humidity Sounder (MHS) have constituted the trace gas product processing system since 2008. The CrIS/Advanced Technology Microwave Sounder (ATMS) processing system has been operational since 2013. Gambacorta et al. [12] compared the accuracy of retrieval products from AIRS/AMSU, IASI/AMSU/MHS and CrIS/ATMS systems using NOAA Center for Satellite Applications and Research (STAR) Operational Hyper Spectral Retrieval Algorithm. Their results showed that the CrIS/ATMS system could provide vertical profiles of atmospheric temperature and water vapor with the same accuracy as those from the other two retrieval systems, except for the temperature in the lower troposphere and the water vapor in the middle troposphere. Under the FSR mode, which enables high spectral resolution of 0.625 cm^{-1} across the full spectral range of CrIS, the vertical profile of carbon monoxide provided by CrIS/ATMS system is comparable in accuracy to the existing carbon monoxide retrievals from AIRS/AMSU and IASI/AMSU/MHS systems. In summary, the CrIS/ATMS processing system already satisfies the requirements for meteorological product retrieval and climate research. The values of CrIS hyper-spectral infrared radiance measurements and their retrieval products in NWP and climate research could be fully realized only when significant improvements in bias correction, quality control and cloud detection and retrieval algorithm for CrIS measurements are made.

注释

① http://nsmc.cma.gov.cn/NewSite/NSMC/Channels/100351.html
② http://www.wmo-sat.info/oscar/instruments/view/93
③ http://www.ozonelayer.noaa.gov/science/basics.htm
④ http://www.nasa.gov/mission_pages/hurricanes/archives/2012/h2012_Sandy.html#4

参考文献

[1] 达成, 邹晓蕾. GOES成像仪资料简介. 气象科技进展, 2014, 4(4): 52-61.
[2] Aumann H H, Chahine M T, Gautier C, et al. AIRS/AMSU/HSB on the Aqua mission: Design, science objectives, data products, and processing systems. IEEE Trans Geosci Remote Sens, 2003, 41: 253-264.
[3] Han Y, Revercomb H, Cromp M, et al. Suomi NPP CrIS measurements, sensor data record algorithm, calibration and validation activities, and record data quality. J Geophys Res Atmos, 2013, 118: 12734-12748.
[4] Strow L L, Motteler H, Tobin D, et al. Spectral calibration and validation of the Cross-track Infrared Sounder (CrIS) on the Suomi NPP satellite. J Geophys Res Atmos, 2013, 118: 12486-12496.
[5] Esplin M, Strow L L, Bingham G, et al. CrIS full spectral resolution test results. 92nd AMS Annual Meeting, New Orleans, LA, January 2012.
[6] Gambacorta A, Barnet C D. Methodology and information content of the NOAA NESDIS operational channel selection for the Cross-Track Infrared Sounder (CrIS). IEEE Trans Geosci Remote Sens, 2013, 51: 3207-3216.
[7] Petty G W. A First Course in Atmospheric Radiation. Madison,

Wisconsin: Sundog Publishing, 2006.
[8] Weng F. Advances in radiative transfer modeling in support of satellite data assimilation. J Atmos Sci, 2007, 64: 3799-3807.
[9] Chen Y, Han Y, Delst P V, et al. Assessment of shortwave infrared sea surface reflection and nonlocal thermodynamic equilibrium effects in the community radiative transfer model using IASI data. J Atmos Oceanic Technol, 2013, 30: 2152-2160.
[10] McNally A P, Watts P D, Smith J A, et al. The assimilation of AIRS radiance data at ECMWF. Q J R Meteorol Soc, 2006, 132: 935-957.
[11] Guidard V, Fourrié N, Brousseau P, et al. Impact of IASI assimilation at global and convective scales and challenges for the assimilation of cloudy scenes. Q J R Meteorol Soc, 2011, 137: 1975-1987.
[12] Gambacorta A, Barnet C D, Wolf W, et al. The NOAA Operational Hyper Spectral Retrieval Algorithm: A cross-comparison among the CrIS, IASI and AIRS processing systems. International TOVS Study Conference. Jeju Island, Korea, March 2014.

附录

已知CrIS瞬时视场中心（P）的经度λ_P、纬度φ_P、仪器波束宽度ω及Suomi NPP卫星（S）天顶角μ_s、方位角φ_s、与地球之间的距离h。将φ_P转换为地心纬度（geocentric latitude）γ_P：

$$\gamma_P = \tan^{-1}[(1-\alpha)^2\tan\varphi_P], \quad (1)$$

式中，α是地球的扁率，它与地球赤道半径（r_a）和极地半径（r_b）的关系为：

$$\alpha = \frac{r_a - r_b}{r_a}。 \quad (2)$$

地球中心由O表示，已知γ_P，可求出O与P之间的距离（d_{OP}）：

$$d_{OP} = (r_a^2\cos^2\gamma_P + r_b^2\sin^2\gamma_P)^{\frac{1}{2}}。 \quad (3)$$

进一步利用λ_P可求出P点在笛卡尔坐标系里的三维坐标即向量$\boldsymbol{OP}$：

$$\boldsymbol{OP} = (x_P, y_P, z_P) = (d_{OP}\cos\gamma_P\cos\lambda_P, d_{OP}\cos\gamma_P\sin\lambda_P, d_{OP}\sin\gamma_P)。 \quad (4)$$

已知d_{OP}、γ_P、μ_s、h，可利用正弦定理求出S与P之间的距离（d_{PS}）：

$$d_{PS} = \frac{(d_{OP}+h)\sin[\mu_S - \arcsin\frac{d_{OP}\sin(\pi-\mu_S)}{(d_{OP}+h)}]}{\sin(\pi-\mu_S)}。 \quad (5)$$

$\boldsymbol{r}_{OP}$为向量$\boldsymbol{OP}$的单位向量，还已知μ_s、φ_s，利用旋转矩阵可求出单位向量$\boldsymbol{r}_{PS}$：

$$\boldsymbol{r}_{PS} = \boldsymbol{R}_{PO}^{\varphi_S}\boldsymbol{R}_{OP\times N}^{\mu_S}\boldsymbol{r}_{OP}, \quad (6)$$

$\boldsymbol{R}_V^\beta$表示将向量绕$\boldsymbol{V}$向量逆时针旋转β度，×表示向量叉乘，$\boldsymbol{N}$表示沿$\boldsymbol{z}$轴方向的单位向量。进一步可求出S点在笛卡尔坐标系里的三维坐标即向量$\boldsymbol{OS}$：

$$\boldsymbol{OS} = (x_S, y_S, z_S) = \boldsymbol{OP} + \boldsymbol{PS} = \boldsymbol{OP} + d_{PS}\boldsymbol{r}_{PS}。 \quad (7)$$

已知向量$\boldsymbol{OS}$、$\boldsymbol{OP}$，可求出向量$\boldsymbol{SP}$和单位向量$\boldsymbol{r}_{SP}$，还已知ω，利用旋转矩阵可求出单位向量$\boldsymbol{r}_{SF_1}$，F_1为瞬时视场轨迹上一点：

$$\boldsymbol{r}_{SF_1} = \boldsymbol{R}_{\boldsymbol{SP}\times\boldsymbol{N}}^{\frac{\omega}{2}}\boldsymbol{r}_{SP}。 \quad (8)$$

S点与$F1$点的距离为d_{SF1}，则：

$$\boldsymbol{SF}_1 = d_{SF_1}\boldsymbol{r}_{SF_1} = (d_{SF_1}x_{SF_1}, d_{SF_1}y_{SF_1}, d_{SF_1}z_{SF_1}), \quad (9)$$

$$\boldsymbol{OF}_1 = \boldsymbol{OS} + \boldsymbol{SF}_1 = (x_S + d_{SF_1}x_{SF_1}, y_S + d_{SF_1}y_{SF_1}, z_S + d_{SF_1}z_{SF_1})。 \quad (10)$$

$F1$点在地球表面，满足椭球体公式：

$$\frac{(x_S + d_{SF_1}x_{SF_1})^2}{r_a^2} + \frac{(y_S + d_{SF_1}y_{SF_1})^2}{r_a^2} + \frac{(z_S + d_{SF_1}z_{SF_1})^2}{r_b^2} = 1。 \quad (11)$$

整理（11），可得：

$$(\frac{x_{SF_1}^2}{r_a^2} + \frac{y_{SF_1}^2}{r_a^2} + \frac{z_{SF_1}^2}{r_b^2})d_{SF_1}^2 + 2(\frac{x_S x_{SF_1}}{r_a^2} + \frac{y_S y_{SF_1}}{r_a^2} + \frac{z_S z_{SF_1}}{r_b^2})d_{SF_1} + (\frac{x_S^2}{r_a^2} + \frac{y_S^2}{r_a^2} + \frac{z_S^2}{r_b^2} - 1) = 0 \quad , \quad (12)$$

式（12）为d_{SF_1}的一元二次方程。若方程有两个不同实数解，取较小值；若方程有两个相同实数解，取该值；若方程无解，则向量$\boldsymbol{OF}_1$不与地球表面相交。进一步可求出F_1的纬度φ_{F_1}和经度λ_{F_1}。利用旋转矩阵将$\boldsymbol{r}_{SF_1}$绕$\boldsymbol{SP}$逆时针旋转ϕ度ϕ=10i，i=1，2，3，…，36）可求出单位向量$\boldsymbol{r}_{SF_i}$：

$$\boldsymbol{r}_{SF_i} = \boldsymbol{R}_{\boldsymbol{SP}}^{\phi}\boldsymbol{r}_{SF_1}。 \quad (13)$$

再根据式（9）—（12）可算出d_{SF_i}，进一步可求出F_i的纬度φ_{F_i}和经度λ_{F_i}。

每9个CrIS瞬时视场组成一个CrIS能视场。每个能视场内，瞬时视场5被称为中心瞬时视场，瞬时视场1、3、7、9被称为对角瞬时视场。已知$\boldsymbol{OS}$、$\boldsymbol{OP}$、$\boldsymbol{OP}_j$（j=1,3,7,9），可求出$\boldsymbol{SP}_5$和$\boldsymbol{SP}_j$，进一步可求出能视场对应的波束宽度θ：

$$\theta = \omega + 2\eta_{\max} \quad (14)$$

$$\eta_{\max} = \max_{j=1,3,7,9}\{\frac{\boldsymbol{SP}_5 \cdot \boldsymbol{SP}_j}{\|\boldsymbol{SP}_5\| \cdot \|\boldsymbol{SP}_j\|}\} \quad (15)$$

已知$\boldsymbol{SP}_5$和θ，可求出单位向量$\boldsymbol{r}_{SP_5}$，再根据式（7）—（12）可求出能视场轨迹F_i^*的纬度$\varphi_{F_i}^*$和经度$\lambda_{F_i}^*$。